

# Design of a Device for the High-Fidelity Haptic Rendering of Rotatory Car Doors

Michael Strolz, Claudia Ehinger and Martin Buss, *Member, IEEE*

**Abstract** — To enable a realistic virtual prototyping of both actuated and unactuated rotatory car doors, a dedicated haptic device is developed. A fundamental issue is the derivation of the specific requirements for this interface, which is done based on knowledge of the typical user interaction with a car door and a comprehensive model of the dynamics of an actuated as well as an unactuated car door. The findings are that the device should only exhibit one rotatory degree-of-freedom, which should be actuated by a direct drive with a high torque output ( $\geq 100Nm$ ) and very high position resolution ( $\geq 16Bit$ ). A suitable direct-drive is selected and combined with other elements to form a backlash-free, very stiff haptic device. Due to both force and acceleration sensing, it can serve for the haptic rendering of actuated as well as unactuated car doors. Furthermore, a thorough safety scheme ensures a safe operation of the human-system-interaction.

**Keywords** — virtual prototyping, robotics, haptic device, haptic rendering, direct drive, actuated mechanisms, car door

## I. INTRODUCTION

In the automotive industry, a major task is to increase the comfort of the access to cars for customers. Besides varying the seat and the shape of the door frame, the haptic properties of the car door are a promising field of research to achieve this goal. Therefore, numerous projects deal with improving them. One approach has been the use of an actuator to influence the dynamics of the car door, see e.g. [1], [2]. This enables the display of different synthesized haptic properties, depending on various sensor data, which has been shown to provide an improved haptic interaction with the car door [3]. Right now, the additional cost of such actuators and sensors prevent these concepts to prevail in car door technology. However, they might be an interesting alternative in the future. Therefore, there is a need for the efficient development of both actuated *and* unactuated rotatory car doors that provide a good haptic interaction.

Many elements contribute to the haptic characteristic of a car door, e.g. its moving mass, door detent, inclination and friction of the joint, the door handles etc. As the “haptic contribution” of the single elements and their interrelation

cannot be seized easily by the designer, it is a difficult task to design and combine them in such a manner that an overall good haptic interaction results. Therefore, the car door design cycle contains many stages of validation, which often includes the use of physical prototypes [4]. These enable evaluations by the designer and by user studies, leading to a better understanding and an improvement of the current design. Unfortunately, the construction of a physical prototype is usually very time consuming, expensive and prone to errors. A promising alternative solution to physical prototyping is “virtual” prototyping [5]: Given a suitable Virtual Reality (VR) test bed, a car door can be simulated multi-modally (haptically, aurally, visually). This enables the car door designer to evaluate the impact of different elements and parameters of the car door on its haptic characteristic. In turn, this can lead to a dramatic acceleration of the design process and, combined with user studies, to an improvement of product quality.

A lot of research has been done on the haptic simulation of virtual objects [6], [7], [8], including the simulation of car doors [9], [10]. However, in the latter approaches only general-purpose haptic devices with more than one DOF were used. While such devices enable a quick display of different car door kinematics, they certainly come with significant compromises in terms of, amongst others, the mechanical stiffness and the actuator selection of the haptic device. This may prevent a very realistic haptic simulation of car doors, limiting the significance of simulation results. In contrast, we intend to develop a dedicated, task-optimized haptic device for the high-fidelity rendering of actuated as well as unactuated car doors with one (rotatory) DOF.

An ideal haptic device displays a virtual object such that the user cannot detect any difference between simulation and reality [11]. To ensure a high degree of this so-called transparency, a variety of requirements have to be met in the design of a haptic device [12]. One major issue is the workspace and the force output capability of the haptic device. Obviously, the simulation of a rotatory car door requires a comparably large workspace ( $> 1m / > 1m^2$ ). Due to the rather hard mechanical constraints of real car doors, very stiff “virtual walls” need to be simulated. Thus, both a large force output capability and a high mechanical stiffness are mandatory.

To achieve a high-fidelity haptic rendering of a car door, the following issues were esteemed to be most critical:

- 1) an end-effector that replicates not only the kinesthetic, but also the tactile properties of the interaction point

Michael Strolz (corresponding author) and Martin Buss are with the Institute of Automatic Control Engineering, Department of Electrical Engineering and Information Technology, Technische Universität München, Munich, Germany (strolz@tum.de, m.buss@ieee.org)

Claudia Ehinger is with the Institute for Machine Tools and Industrial Management, Department of Mechanical Engineering, Technische Universität München, Munich, Germany (claudia.ehinger@iwb.tum.de)

This work was supported in part by BMW Group in the framework of CAR@TUM.

- 2) an accurate, high-bandwidth measurement of the user interaction force
- 3) a high-bandwidth force or motion control of the haptic device, including:
  - fast computation and output of actuation signals
  - small actuator dynamics
  - high mechanical stiffness in the rotational DOF
  - very high stiffness in all other directions
- 4) a very accurate dynamic model of the car door

The requirements (1) and (2) can rather easily be achieved by using parts of a conventional car door handle and mounting them rigidly to an appropriate force sensor. In contrast, modeling the car door accurately, deriving the specific requirements for the design of the haptic device and ultimately designing it properly is much harder.

In the following, we solve these problems and design a haptic device that indeed enables the high-fidelity rendering of a car door with one DOF.

## II. PERFORMANCE SPECIFICATION OF THE HAPTIC DEVICE

To build a high-fidelity haptic device, an accurate performance specification is mandatory to identify the main requirements that have to be met. This in turn necessitates knowledge about the dynamics that have to be simulated and of the human user who will interact with them. In the following, we model the user interaction at a car door and the dynamics of both an unactuated and an actuated car door. From these models, we derive the the performance specification for the design of the haptic device.

### A. User Interaction at a Car Door

We performed various tests and measurements to assess the haptic interaction between a car door and the human user. In our setup, it turned out that the maximum force exerted by the user,  $f_{U,max}$ , predominantly is below 90N (see Fig. 4 for a typical interaction). Such large forces are exclusively applied at the outer rim or upper corner of the door when the user closes the door with a push. This means that the worst-case moment of force exerted by the user is

$$\tau_{U,max} = f_{U,max} \times r_{max} \approx 100Nm \quad (1)$$

for long car doors<sup>1</sup>.

Kinesthetic interaction usually involves frequencies below 20Hz [13]. We assume that this holds for the usual interaction of a human with a car door<sup>2</sup>. This assumption is backed by the power spectra of force and position measurements of our experiments on typical interaction scenarios at car doors.

<sup>1</sup>Assumption about maximum perpendicular distance between hinge and interaction point at car door:  $r_{max} = 1.1m$ .

<sup>2</sup>Of course, especially when closing the door with a push, much higher frequencies can be involved due to an impact, but then the user may let the door loose such that there is no haptic interaction anymore.

### B. General Modeling and Control Issues

A realistic simulation of the haptic interaction with an actuated or unactuated car door requires a detailed dynamic model to describe the one DOF rotational movement. One way to build this model is to consider all the haptically relevant properties and sub-elements of the door as an impedance, resulting in an *internal* torque  $\tau_{door,i}$ :

$$\begin{aligned} \tau_{door,i} = & \tau_G(\varphi, \theta, \xi) + \tau_F(\dot{\varphi}, \varphi) + \tau_D(\dot{\varphi}, \varphi) + \\ & \tau_V(\dot{\varphi}, \varphi) + \tau_P(\dot{\varphi}, \varphi) + \tau_E(\dot{\varphi}, \varphi) + \\ & \tau_A(\dot{\varphi}, \varphi, \tau_{door,e}, t) + \tau_{r,i}(\dot{\varphi}, \varphi) \end{aligned} \quad (2)$$

where  $\varphi$  is the rotatory DOF,  $\tau_G(\varphi, \theta, \xi)$  is the gravitational component resulting from the inclination ( $\theta, \xi$ ) of the hinge relative to gravity,  $\tau_F(\dot{\varphi}, \varphi)$  is the torque resulting from the friction in the door hinge,  $\tau_D(\dot{\varphi}, \varphi)$ ,  $\tau_V(\dot{\varphi}, \varphi)$  and  $\tau_P(\dot{\varphi}, \varphi)$  are the contributions of the detent, the air ventilation and the packing of the door,  $\tau_E(\dot{\varphi}, \varphi)$  is the resisting torque of the mechanical end positioning elements,  $\tau_A(\dot{\varphi}, \varphi, \tau_{door,e}, t)$  is the torque exerted by an optional actuator, and  $\tau_{r,i}(\dot{\varphi}, \varphi)$  are residual internal effects. The *external* torque is given by

$$\tau_{door,e} = \tau_U(t) + \tau_W(\dot{\varphi}, \varphi, t) + \tau_{r,e}(\dot{\varphi}, \varphi, t) \quad (3)$$

where  $\tau_U(t)$  is the user interaction torque,  $\tau_W(\dot{\varphi}, \varphi, t)$  is the torque exerted by wind and  $\tau_{r,e}(\dot{\varphi}, \varphi, t)$  are residual external effects. In the following,  $\sum \tau = \tau_{door,i} + \tau_{door,e}$  denotes the sum of all torques that act on the rotational DOF of the car door. Modeling errors and disturbances will be neglected ( $\tau_{r,i} = \tau_{r,e} = \tau_W = 0$ ,  $\tau_{door,e} = \tau_U(t)$ ).

The dynamics of the car door is given by  $\sum \tau = \ddot{\varphi} I_{zz}$ , where  $I_{zz}$  is the inertia of the car door related to the rotational hinge.

The car door can be simulated by an impedance or an admittance model. Admittance control would require the calculation of the reference acceleration  $\ddot{\varphi}_{ref}$  of the car door based on the state ( $\dot{\varphi}, \varphi$ ) and the measurement of user interaction as

$$\ddot{\varphi}_{ref} = (\tau_{door,i}(\dot{\varphi}, \varphi, \tau_U, t, \theta, \xi) + \tau_U(t)) / I_{zz} \quad (4)$$

Impedance control would require the measurement of the state ( $\dot{\varphi}, \varphi$ ) to get the reference user interaction torque  $\tau_{ref}$ .

It is well known that the stability of admittance control and impedance control is complementary, see e.g. [14]: While it is hard to render a low mass and damping stably by an admittance control scheme, impedance control can not provide stability for infinitely stiff contacts. As rotatory car doors exhibit a comparatively high inertia, admittance control should work quite stable (at least if appropriate hardware is used). At the same time, in contrast to impedance control it enables to realistically render the hard mechanical constraints that car doors exhibit. Thus, and because of its ability to counteract unmodeled dynamics of the haptic device, we prefer admittance control for the rendering of car doors.

In the following, we model  $\tau_{door,i}$  based on experimental identification, resulting in part in look-up tables.

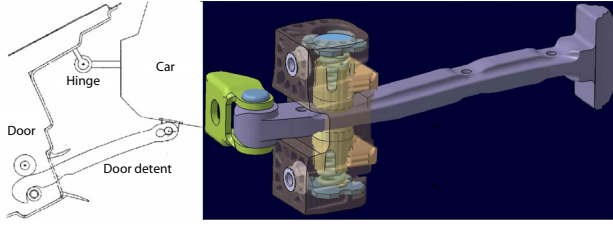


Fig. 1. Location (l.) and mechanical scheme (r.) of the door detent

### C. Dynamics of a Conventional Unactuated Car Door

First, we consider a conventional car door which is produced in a large scale at BMW AG. It is not actuated, thus  $\tau_A = 0$ .

1) *Gravity*: In general, the door hinge is not aligned with the effective direction of gravity. It exhibits an inclination ( $\theta$ ,  $\xi$ ) that depends both on the construction of the door hinge and the tilt of the car body. This results in a gravitational torque  $\tau_G$ , which acts to minimize the potential energy. To model this torque, we calculate the shortest distance between the center of gravity (CG) and the rotational axis, which gives the lever  $l_{CG}$ . From this, we can derive the effective lever for gravity,  $l_{eff} = l_{CG} \cdot \cos(\frac{\pi}{2} - \theta - \xi)$ , and then calculate the gravity torque:

$$\tau_G(\varphi, \theta, \xi) = mg \cdot l_{eff}(\varphi, \xi) \cdot \sin(\theta) \quad (5)$$

2) *Friction*: The door hinge exhibits several friction effects. Measurements revealed that the dry friction  $\tau_{F,D}$  is predominant, while the static friction  $\tau_{F,S}$  plays only a minor role. The friction can easily be modeled as a constant for every simulation step  $k$ :

If  $\dot{\varphi}_{k-1} = 0$  and  $|\sum \tau_k - \tau_F(\dot{\varphi}, \varphi)_k| > |\tau_{F,S}|$ , or if  $\dot{\varphi}_{k-1} \neq 0$  and  $|\sum \tau_k - \tau_F(\dot{\varphi}, \varphi)_k| > |\tau_{F,D}|$ , the door will move, thus  $\tau_{F,k} = \tau_{F,D}$  and  $\dot{\varphi}_k \neq 0$ . Else, the door will not move, thus  $\dot{\varphi}_k = 0$  and  $\varphi_k = \varphi_{k-1}$ .

3) *Door detent*: The door detent is located between the door and the front pillar of the car, as can be seen in Fig. 1. It is a mechanical component which is meant to bring an open car door in one of three rest positions, thereby holding the door even at moderate inclinations to provide a comfortable access to the car. This is achieved by means of a combination of a spring and a mechanical profile, resulting in a characteristic torque  $\tau_D$  which is depicted in Fig. 2.

Friction effects (mainly dry friction) account for different  $\tau_D$  when opening and closing, which can be seen by comparing them to the mean value (solid line). Accordingly, the door detent has been modeled as a separate look-up table for both movement directions.

4) *Air ventilation*: While the aerodynamic drag of the car door is negligible, the influence of the air ventilation of the car is not: Especially when the door is opened or closed with a high velocity ( $\dot{x} > 0.5 \frac{rad}{s}$ ) at the external door handle, the resisting torque  $\tau_V(\dot{\varphi}, \varphi)$  resulting from the decompression or compression of the air inside the car is significant.

For sake of simplicity, in the following we assume that all car doors and all windows are fully closed, which gives

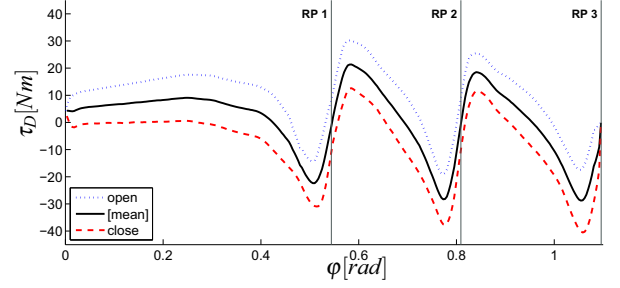


Fig. 2. Measurement of the door detent torque  $\tau_D$  while opening and closing the door with constant velocity  $\dot{\varphi}$ . From the mean value (solid line) it can easily be seen that the detent provides three rest positions (RP) for placing the door.

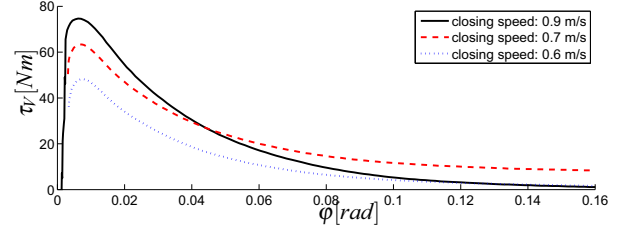


Fig. 3. Measurements of the air ventilation torque  $\tau_V$  for different, constant closing speeds  $\dot{\varphi}$ .

the  $\tau_{V,max}(\dot{\varphi}, \varphi)$ . As soon as the car door presses against the rubber packing, the compressed air can only vanish through the ventilation slots of the car. Thereby, the design of air ventilation has a strong influence on the dynamics of the car door, especially for large velocities.

To quantify this effect, the pressure  $p(\dot{\varphi}, \varphi)$  within the car was measured while the door was closed with different velocities  $\dot{\varphi}$ . We assume that the pressure acts homogeneously on the inner surface area  $A$  of the car door, whose center exhibits a perpendicular distance  $r_A$  to the hinge axes. Accordingly, we model the effective torque caused by air compression/decompression as

$$\tau_V = p(\dot{\varphi}, \varphi) A \times r_A \quad (6)$$

This enabled an experimental identification: For different constant velocities  $\dot{x}$ , we measured  $p$  and  $\varphi$ . From these measurements, which partly are displayed in Fig. 3, we built a look-up table for  $\tau_V$ .

5) *Rubber Packing*: The car door protects the driver not only from collision impacts, but also from precipitation and noise. By effectively sealing the door, a rubber packing accounts for this. Towards the car door, the packing acts like a nonlinear spring with  $\tau_P$  depending heavily on position and mildly on velocity. Thus, the identification was done by measuring the static force at the external door handle for different  $\varphi$ .

6) *Maximum opening angle*: There is a so-called ‘‘maximum’’ opening angle  $\varphi_{max}$  for the car door. Larger angles are counteracted by mechanical end positioning elements, which exhibit a spring-like behavior. The spring constant was determined by applying a constant torque on the car door and measuring the corresponding angle.

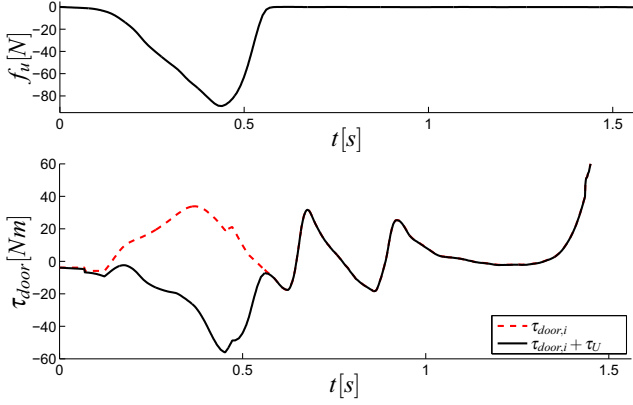


Fig. 4. Typical user interaction force  $f_u = \tau_u/r$  (above) and calculated resulting torques  $\tau_{door,i}$  and  $\tau_{door,i} + \tau_U$  (below) when closing the car door with a slap (reference for the validation of the door model)

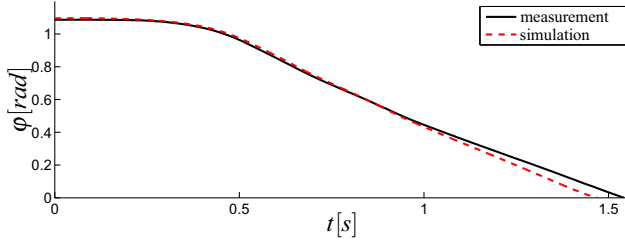


Fig. 5. Motion of the car door when applying a typical force (see Fig. 4): Measurement (solid line, corresponding to  $f_U$ ) and simulation (dashed line, corresponding to the calculated torque  $\tau_{door,i} + \tau_U$ )

7) *Validation of the door model:* To validate the model of the car door, we performed an experiment in which the fully-opened car door was closed by a human rapidly. The force applied by the user as well as the resulting door model torques are depicted in Fig. 4. The force leads to a motion of the car door which can be seen in Fig. 5 (solid line). We used this force as input for the admittance model of the car door, which resulted in a simulated motion that can also be seen in Fig. 5 (dashed line).

Though the simulated and the measured motion are very close for a significant time, they differ at the end of the closing process. Obviously, the force measurement can not be responsible for this deviation, as it occurred more than 0.2s after the force signal settled at zero. Thus, we think that modeling errors of mainly two effects contribute to this errors: the static friction  $\tau_{F,S}$ , where we assumed  $\dot{\phi} = 0$ , and the air ventilation  $\tau_V$ , where we assumed a homogeneous distribution of the pressure. Further efforts will be undertaken to achieve a more realistic model.

Nonetheless, we believe that the dynamic model of the car door presented here is realistic enough to derive quantitative metrics for the performance specification of the haptic device.

#### D. Dynamics of an Actuated Car Door

If a car door is to be enhanced by an actuator and its control software and hardware, it may also be haptically rendered. As a framework for simulating controlled mechanisms, Active Admittance Control has been introduced by

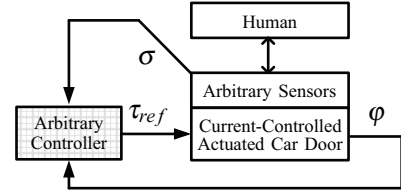


Fig. 6. General control scheme of an actuated car door. Based on a measurement of the angle  $\phi$  and other sensor signals  $\sigma$  (e.g. interaction force, switches, etc.), a reference torque  $\tau_{ref}$  is calculated and applied to the current-controlled door.

Strolz and Buss [10]. The basic approach is to include a model of the controller, the signal processing and the actuation hardware in the simulation of an actuated mechanism. In Active Admittance Control, the actuation torque  $\tau_A$  acts in parallel with the measured human interaction torque  $\tau_U$  on a model of the mechanic structure. For a car door, the reference motion can be calculated according to (2) and in turn be displayed by a motion-controlled haptic device.

An interesting question is now, which dynamics an actuated car door exhibits and what this means for the design of the a haptic device.

Let us consider a current-controlled, actuated car door and its controller as depicted in Fig. 6, where  $\tau_M = \tau_{door,i} - \tau_A$  represents the mechanical component of the internal torque of the door. As a realistic hardware example, the actuation introduced in [3] is used. It consists of a DC motor with a planetary drive and a spindle. Due to a large transmission factor, the inertia of the planetary drive and especially the DC motor significantly increases the overall inertia of the door. Furthermore, as is pointed out in [3], the actuation exhibits a Coulomb and viscous friction. Thus, there is a significant difference in the mechanical parameters of both models:

$$I_{ZZ,act} \gg I_{ZZ,unact}, \quad \tau_{F,act} \gg \tau_{F,unact} \quad (7)$$

Due to its higher impedance, the mechanical model of the actuated car door can easier be rendered in admittance display mode then the unactuated car door. But what about the overall dynamics of the current-controlled door?

If the controller depicted in Fig. 6 calculates a step  $\Delta\tau_{ref}$  in the reference signal  $\tau_{ref}$ , this directly leads to a step in the reference current  $\Delta I_{ref}$ . Due to the typically high bandwidth of the closed-loop current control of the actuator (e.g.  $\omega_0 \approx 1.3kHz$ ,  $T_{el} = 1.29ms$  for the one described in [3]), the reference  $\Delta I_{ref}$  leads to a fast step response acting on the user.

#### E. Specific Requirements

The main requirements for the haptic device and, in particular, its drive lay in the areas current-control bandwidth, mechanical properties, torque output, and motion measurement.

1) *Current-control bandwidth:* A realistic simulation in admittance display mode requires a step in the reference acceleration to be propagated to the current-controller of the haptic device. A typical PD position controller would not

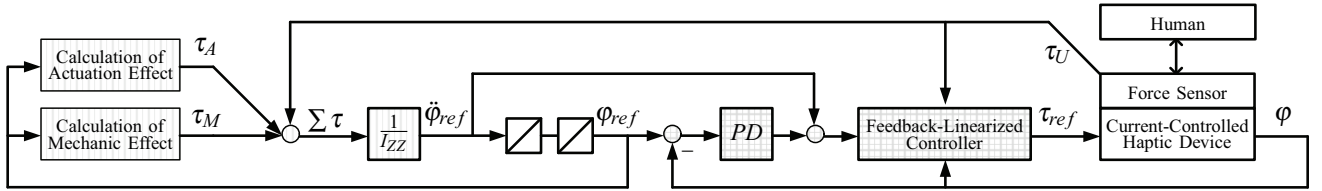


Fig. 7. Advanced control scheme for the haptic rendering of rotary car doors with acceleration-feedforward and feedback-linearization. If no actuation is to be included in the simulation,  $\tau_{d,A} = 0$ .

be suitable for this, because the step would be significantly shaped by a rather slow motion control loop (typical:  $\omega_0 \leq 50\text{Hz}$ ). Rather, a feedforward control has to be used. We propose the advanced control scheme shown in Fig. 7. Based on (4), the reference acceleration  $\ddot{\phi}_{ref}$  is calculated. It is tracked by a PD position controller with acceleration feedforward. Additionally, a feedback compensation linearizes the current-controlled plant. Thus, a relatively stiff position control can be realized (see also [15]).

Which conditions have to be satisfied in order that the effective acceleration  $\ddot{\phi}$  caused by  $\Delta\tau_{ref}$  is rather the same for reality (Fig. 6) and simulation (Fig. 7)? Obviously, the closed current-control loop of the haptic device should not be slower than that of the actuated door. However, if the actuated car door exhibits much more damping (due to friction) than the drive of the haptic device, this condition can be relaxed.

We deemed a lower limit of  $500\text{Hz}$  for the current-control bandwidth to be appropriate.

2) *Maximum speed*: According to measurements, the maximum speed of the tip of the car door is  $\approx 4\frac{m}{s}$  in world coordinates. It occurs when the user applies a force at the very end of the door, thus when  $r > 0.8m$ . This means that the maximum rotational speed  $\dot{\phi}_{max}$  that has to be displayed by the haptic device is  $\dot{\phi}_{max} < 5\frac{rad}{s} < 1RPS$ .

3) *Maximum torque output*: The peak torque output capability of the drive, denoted by  $\tau_{max}$ , has to be at least  $100Nm$  to compensate  $\tau_U$  if necessary. However, such a high torque has to be displayed for a very short time only ( $t_{\tau_{max}} < 0.1s$ ), so the rated torque may be considerably smaller. Note that  $\tau_{max}$  should not be exceedingly high, because it diminishes safety. Thus, a compromise has to be found. For our case, we considered an upper bound of  $150Nm$  as appropriate.

4) *Necessity to use a direct drive*: For many applications, including haptic rendering, rather high torques and low velocities are desired when compared to the properties of electric motors. Thus, usually gearboxes between motor and load (often with transmission rates  $\gg 1$ ) are used to adapt these properties accordingly. Unfortunately, they introduce additional dynamics to the system. Depending on the respective gear concept, the most significant effects may be backlash, elasticity and/or friction. Each of these effects can be detrimental for realistic haptic rendering.

In many practical haptic scenarios, only minor forces/torques ( $\leq 10N/\leq 1Nm$ ) have to be displayed to the user. This means, that the influence of the physical elasticity of the gear may not be perceptible to the user, which allows the use of “zero-backlash” gears like the

well-known Harmonic Drives. However, in our scenario  $100Nm \leq \tau_{max} \leq 150Nm$  is required. If we used a rather elastic gearbox, this torque would cause a significant contortion between end-effector and drive, immediately destroying the haptic illusion. If we used a gearbox which exhibits backlash, this backlash would become noticeable due to the long rod. Therefore, the use of a gearbox would inhibit high-fidelity haptic rendering, so the best way was to pass on a transmission and couple the load directly to the motor, which then is called a “Direct Drive” (DD). Previous research has shown that DD are suitable for achieving a high-fidelity control of a robot, see e.g. [16], [17]. While different types of motors can be used as a DD, the most common one is the brushless permanent magnet synchronous motor (PMSM, “brushless DC”). Such PMSM-DD usually provide a very good dynamic response due to a small electrical time constant and the “missing” mechanical transmission components, as well as high torque at stall.

5) *Configuration*: PMSM-DD are available in two configurations: “frameless” and “standalone”. If the motor should be an integral part of the device (which is often the case for machine tools), the motor should be delivered “frameless”, thus without housing and bearing. This means that the machine designer has to take care of the integration, which contains aspects like providing sufficient heat dissipation, selecting an appropriate feedback device and to achieve a stiff construction with low friction. In contrast, “standalone” motors are complete servo motors which can directly be mounted on the load. They come in part with very stable bearings which resist more than the load we require. This is a key advantage, because then there is no need for mounting an external bearing, which would be prone to introduce backlash and unknown friction to the drive. Therefore, it is desirable to use a “standalone” DD with a sufficiently stable bearing.

6) *Mechanical rigidity*: A high-fidelity rendering of a car door requires a very stiff display of all non-simulated DOF. As every DOF of a robot introduces additional elasticities, amongst other detrimental effects, this motivates to build a robot with only one rotational DOF. This requires that the DOF exhibits the same orientation as the hinge of the simulated car door. Furthermore, it should be possible to use various interaction points and adequate end-effectors, e.g. the outer or the inner door handle. This can be achieved by mounting a stiff rod with a length  $r_{rod} = 1.1m$  on a rotational drive, enabling the rendering of even very long doors. Various end-effectors can then be attached to the rod

TABLE I  
OVERVIEW OF SOME INTERESTING ROTATIONAL DIRECT DRIVES FOR HIGH-FIDELITY HAPTIC RENDERING

	Units	Min. Requ.	Danaher M. DH101A S600	NSK YSB5120 M-ESB-YSB...	Parker 190ST2M C3S150V4	Parker DR5300A DR5000A	YASKAWA SGMCS-80M SGDH-15AE
Max. Torque	$Nm$	$\geq 100$	120	120	119	300	240
Max. Rotational Speed	RPS	$\geq 1$	5.0	3	8.3	5.0	5.0
Position Resolution	$bit$	$> 15$	20	$\approx 20$	16	$\approx 19$	20
Abs. Positioning Acc.	$arc\ sec$	-	$\pm 27$	$\pm 150$	$\pm 600$	$\pm 45$	$\pm 15$
Repeatability	$arc\ sec$	-	$\pm 1.2$	$\pm 1.6$		$\pm 5.0$	$\pm 1.3$
Max. Axial Load	$N$	$\geq 500$	52000	19600	25000	3991	9000
Max. Moment Load	$Nm$	$\geq 100$	437	400		20	180
Inertia	$kg\ m^2$	$\leq 1$	0.069		0.010	0.340	0.063

to simulate different interaction points.

The rod and the drive should withstand at least moderate unwanted forces exerted by the user orthogonally to the DOF. If e.g.  $f_U = 20N$  acts at the very end of the rod, this causes an axial load of  $f_L = (m_{rod} + m_{ee})g + f_U < 100N$  and a moment load of  $\tau_L = 220Nm$ , as can be seen in Fig. 8.

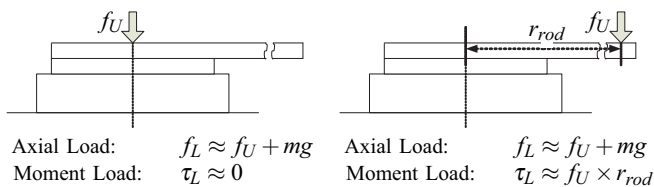


Fig. 8. Axial and moment load working on a drive

7) *Position measurement*: According to [18], humans have a spatial resolution of up to  $5\mu m$ . Given a maximum lever length of  $1.1m$ , an ideal haptic device would therefore require at least a positioning accuracy and repeatability of  $< 1arcsec$  and thus a position resolution of  $\gg 20Bit$ . For our case, a lower rotational resolution of about  $16Bit$  should be sufficient, because the handling of a car door does not involve precise positioning. However, a higher resolution enables a higher angular stiffness of the motion-controlled direct drives, thus resolutions of up to  $20Bit$  are recommended [19].

### III. DESIGN OF THE HAPTIC DEVICE

Based on the performance specification, a suitable PMSM-DD had to be mounted and installed such that a safe, high-performance haptic device could be achieved.

#### A. Selection of a Suitable Direct Drive

It was a surprisingly difficult task to find a DD that fulfilled the requirements which are in part summarized in Table I. DDs still seem to be a specialty that comparatively few manufacturers offer. Many otherwise interesting PMSM-DDs (e.g. ALXION 145 STK or Intellidrives SRT-67) were not available in a standalone configuration. Furthermore, most of the motors come with either far to low or far to high torques, so  $\tau_{max}$  was also a major constraints. Other issues were the position resolution and the maximum moment load.

We identified five reasonably relevant PMSM-DD, which may also be of interest for other haptic applications:

The DH101A of Danaher Motion [20], the YSB5120 of NSK [21], the 190ST2M and the DR5300A of Parker [22], [23] and the SGMCS-80M of YASKAWA [24]. They are denoted with the name of their respective driver unit (DU, frequency converter) and their most fundamental properties in Table I.

Obviously, the DR5300A and the SGMCS-80M ( $240Nm \gg 150Nm$ ) do not fully meet our requirements, whereas the three others do. While contacting the manufacturers, we learned that the 190ST2M exhibits a superb low friction and a very low torque ripple. Therefore, we chose the 190ST2M despite the fact that the other two alternatives might have provided a similar behavior.

#### B. Safety Concept

The haptic device was designed to ensure a safe operation. This is especially important when people with no professional background operate the haptic device, e.g. during user studies. Both hardware and software based precautions have been implemented.

1) *Mechanical bounds*: One important safety measure is to constrain the motion of the device such that only the necessary workspace is left. This can easily be achieved by a mechanical construction, where firmly mounted horizontal beams at  $\varphi_{min}$  and  $\varphi_{max}$  provide safe bounds that hold when the maximum acceleration is applied.

2) *Braking*: In case of any fault or emergency, the movement of the direct drive has to be stopped immediately, which requires the use of a brake. It is the most important safety measure and has to conform to several requirements:

- The braking torque  $\tau_{BR}$  must be higher than the maximum torque output of the direct drive,  $\tau_{DD,max}$ .
- The full braking must be performed fast. We defined the upper bounds  $0.05s$  and  $0.02\pi$ .
- The mechanics of the brake should not be detrimental to the stiff and backlash-free rest of the actuated DOF.

We found a suitable electro-magnetic brake for our application, which consists of an encapsulated coil, an fixed friction lining and an armature assembly with armature plate and pre-stressed spring [25]. The armature assembly is connected to the shaft of the direct drive. If the supply voltage is applied, a magnetic field attracting the armature plate is generated. The contact between this plate and the frictional surface of

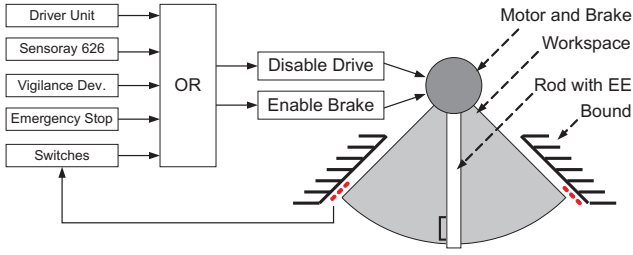


Fig. 9. Safety measures for the operation of the haptic device

the stator then causes braking. If the voltage is removed, the pre-stressed spring pulls the armature plate back, thereby braking ends.

Based on the worst case data of our application, we calculated the braking time  $t_{stop}$ , which is the sum of the response delay time  $t_d$ , the rise time  $t_r$  and the slipping time  $t_s$  of the brake. With the use of an additional high-speed switchgear, enabling high-speed excitation of the DC voltage coils,  $t_d$  and  $t_r$  can be reduced to 10% of the values given in [25].  $t_s$  is approximated as follows [25]:

$$t_s = \frac{I \cdot n}{9.55(\tau_{BR} - \tau_{DD,max})} + \frac{t_r}{2} \quad (8)$$

where  $I$  is the inertia of the moving mechanism,  $n$  is the rotational speed of the motor,  $\tau_{BR}$  is the braking torque and  $\tau_{DD,max}$  is the maximum torque of the direct drive. This gives the braking time  $t_{stop} \approx 45ms$ . Thus, given the maximum speed  $\dot{\varphi}_{max} < 1RPS$  derived in Sec. II-E.2, the requirements were met.

3) *Emergency sensors*: Two mechanical switches are used to monitor the beginning and the end of the predefined rendering space  $0 \leq \varphi \leq 0.4\pi$ . If the device exceeds this space, they cause a full-stop-braking of the device.

Additionally, an automatic vigilance device as well as an emergency stop switch are provided to ensure the possibility of manual emergency braking.

4) *Software*: In addition to the safety precautions referring to the wiring and the mechanical design software measures ensure a quick and safe reaction to faults. Software precautions can be undertaken on the one hand by adjusting the settings of the driver unit (DU) of the direct drive and on the other hand by the integration of safety blocks in the Simulink model.

In the configuration settings of the DU the maximum torque and the maximum speed can be limited. Additionally, occurring overload and over-temperature are detected and cause a fault. This disables the input  $ENABLE\_IN$  of the DU, which is connected in series with the switches, the automatic vigilance device<sup>3</sup> as well as an emergency stop switch. This triggers emergency braking, as can be seen in Fig. 9. Furthermore, it disables the power stage of the DU.

The status flags of the driver unit and the sensor signals are connected to a PC run by RTAI Linux (hard real-

<sup>3</sup>An automatic vigilance device has a button which has to be pressed by the user in a specific way. If it is pressed too soft or too hard, a signal is emitted, which is utilized as emergency stop.

time operating system). There, via the PCI-based I/O-card Sensoray626, the flags are read into the Simulink model, where they are also monitored. If one of the limits is exceeded or the status is incorrect, emergency braking is triggered.

Additionally, the output signal of the model is limited, so that it cannot exceed the maximum permissible value.

### C. Motion and Force Sensors

As already mentioned, a high-quality motion and force feedback is essential to achieve high-fidelity haptic rendering. Besides the built-in high resolution resolver, a Ferraris-type acceleration sensor was mounted on the shaft of the direct drive to measure the acceleration of the motor. During the movement, the permanent magnets of the detector induce eddy currents in the bell-shaped rotor. The eddy currents are proportional to the radial velocity. Every change of the eddy currents and therefore every change of the radial velocity induces a voltage in the coils of the detector, which is proportional to the radial acceleration [26], [27]. The acceleration signal enables e.g. the use of a Kalman filter for a better determination of the velocity  $\dot{\varphi}$ .

To implement an admittance control loop a precise signal of the interaction force is needed. The sensor should detect static and dynamic forces up to 200N precisely and with high linearity. The chosen sensor [28] can easily be mounted between the end of the rod and the door handle.

### D. Mechanical Construction

To achieve a high fidelity haptic rendering the haptic device has to be as stiff as possible. Therefore it is mounted on a stiff baseplate on the ground and only stiff material is used for its construction. All plates are made out of steel, whereas the material of the cross beams and the rod is aluminum. All following mechanical components had to be integrated in the mechanical design in such a manner that their function is not disturbed and that they easily can be assembled and disassembled: direct drive, acceleration sensor, brake, rod, force sensor and door handle. Because of their low tolerances, especially the acceleration sensor and the brake had to be mounted carefully. As already mentioned in Sec. III-B.1, two vertical beams are provided to prevent the motor from uncontrolled rotational movement. Additionally, a horizontal beam safeguards the bearing of the PMSM-DD against impermissible moment load.

The realized construction is displayed in Fig. 10. The left picture shows the drive and the attached elements in detail, while the right picture shows the whole setup including the safety construction and the end-effector with the force sensor.

## IV. CONCLUSION AND FUTURE WORKS

In this paper, we describe how we met the requirements of a haptic device that enables the high-fidelity rendering of car doors with one rotatory DOF. The most important part is to derive the specific requirements for the design of such a task-optimized device. This is done based on a



Fig. 10. Setup of the high-fidelity haptic device for car door simulations, featuring a direct drive ( $\tau_{max} = 100Nm$ ) and an outer door handle as end-effector (l: drive, rod, and brake; r: whole setup)

comprehensive model of both the user and the dynamics both an actuated and unactuated door, which is gained and validated by extensive experimental identification as well as theoretical considerations.

We found out that the device should consist of one direct drive with high torque output ( $\geq 100Nm$ ) and very precise position resolution ( $\geq 16Bit$ ). Only few direct drives that meet our requirements are available on the market. They were compared and discussed. The selected drive was combined with other elements to form a backlash-free, very stiff haptic device on which various end-effectors as e.g. an outer door handle can be mounted. Its high torque output makes the device potentially very dangerous. Hence, a thorough safety concept containing both hardware and software components has been developed and realized. A Ferraris-type acceleration sensor and a force sensor have been integrated in the haptic device to enable both a high-quality admittance and impedance control.

In the future, we will implement the haptic control scheme given by Fig. 7. Based on the accurate model of the actuated or unactuated car door, it is promising to provide a very realistic simulation on the haptic device. In an experiment, human users will compare this simulation with a physical instance of the car door, such that a quantitative measure for the quality of the haptic rendering can be derived.

## V. ACKNOWLEDGEMENTS

The authors wish to thank Florian Soldner of BMW AG for his valuable help in identifying the dynamics of a conventional, rotatory car door.

## REFERENCES

- [1] J. Maas and S. Kern. Mechatronic vehicle door assistant. In *IEEE/ASME International Conference on Advanced Intelligent Mechatronics*, pages 1–5, 2007.
- [2] N. Tomohiko and S. Hiroyuki. Opening and closing device of door for vehicle. JP05112128A, 1993.
- [3] M. Strolz, A. Mörtl, M. Gräf, and M. Buss. Control of an actuated car door providing outstanding haptic interaction. In *Proceedings of Third Joint Eurohaptics Conference and Symposium on Haptic Interfaces for Virtual Environment and Teleoperator Systems (World Haptics 2009)*, Salt Lake City, UT, USA, March 18–20 2009.

- [4] VDI-EKV. *Design methodology for mechatronic systems (VDI-Richtlinie 2206)*. Verein Deutscher Ingenieure, 2004.
- [5] A.B. Garcia, R.P. Gocke, and N.P. Johnson. Virtual prototyping: Concept to production. Technical report, Defense Systems Management College, 1994.
- [6] C.L. Clover, G.R. Luecke, J.J. Troy, and W.A. McNeely. Dynamic simulation of virtual mechanisms with haptic feedback using industrial robotics equipment. In *Proceedings of the IEEE International Conference on Robotics and Automation (ICRA 1997)*, volume 1, pages 724–730, 1997.
- [7] P.U. Lee, D.C. Ruspini, and O. Khatib. Dynamic simulation of interactive robotic environment. In *Proceedings of the IEEE International Conference on Robotics and Automation (ICRA 1994)*, number 2, pages 1147–1152, 1994.
- [8] A. Nahvi, D.D. Nelson, J.M. Hollerbach, and D.E. Johnson. Haptic manipulation of virtual mechanisms from mechanical CAD designs. In *Proceedings of the IEEE International Conference on Robotics and Automation (ICRA 1998)*, volume 1, pages 375–380, 1998.
- [9] P. Buttolo, P. Stewart, and A. Marsan. A haptic hybrid controller for virtual prototyping of vehicle mechanisms. In *Proceedings of the 10th Symposium on Haptic Interfaces for Virtual Environment and Teleoperator Systems*, pages 249–254, 2002.
- [10] M. Strolz and M. Buss. Haptic rendering of actuated mechanisms by active admittance control. In Manuel Ferre, editor, *Haptics: Perception, Devices and Scenarios*, volume 5024 of *LNCS*, pages 712–717. Springer, 2008.
- [11] R.J. Adams and B. Hannaford. Control law design for haptic interfaces to virtual reality. *IEEE Trans. on Control Systems Technology*, 10(1):3–13, 2002.
- [12] M. Ueberle, N. Mock, and M. Buss. ViSHaRD10, a novel hyper-redundant haptic interface. In *Proceedings of the 12th International Symposium on Haptic Interfaces for Virtual Environment and Teleoperator Systems*, pages 58–65, 27–28 March 2004.
- [13] T.L. Brooks. Telerobotic response requirements. In *IEEE International Conference on Systems, Man and Cybernetics*, pages 113–120, 1990.
- [14] J. Hoogen and G. Schmidt. Complementary control architectures for haptic displays. *at - Automatisierungstechnik*, 54(1):1–9, January 2006.
- [15] M. Ueberle. *Design, Control, and Evaluation of a Family of Kinesthetic Haptic Interfaces*. PhD thesis, TU München, 2006.
- [16] S.D. Eppinger and W. Seering. Understanding bandwidth limitations in robot force control. In *Proceedings of the IEEE International Conference on Robotics and Automation*, volume 4, pages 904–909, 1987.
- [17] S.D. Eppinger and W.P. Seering. Three dynamic problems in robot force control. *IEEE Transactions on Robotics and Automation*, 8(6):751–758, 1992.
- [18] L.A. Jones and I.W. Hunter. Differential thresholds for limb movement measured using adaptive techniques. *Perception & Psychophysics*, 52(4):529–535, 1992.
- [19] A. Holzknrecht. Direct drive torque motors for machine tool applications. Technical report, ETEL S.A., 2002.
- [20] Danaher Motion, 203A West Rock Road, Radford, VA 24141, USA. *KOLLMORGEN GOLDLINE DDR*, 2007.
- [21] NSK Ltd., Tokyo, Japan. *Direct Drive YSB Series*, 2002.
- [22] Parker Hannifin Corporation, Electromechanical Automation Division, 5500 Business Park Drive, Rohnert Park, CA 94928, USA. *Catalog 8000-4/USA, Dynaserv Series*, 2007.
- [23] Parker Hannifin Corporation, Electromechanical Automation Division, 5500 Business Park Drive, Rohnert Park, CA 94928, USA. *Torque Motors ST Direct Drive Servomotors*, March 2008.
- [24] YASKAWA ELECTRIC CORPORATION, 2121 Norman Drive South, Waukegan, IL 60085, USA. *Direct Drive Sigma Series*, November 2007.
- [25] INTORQ GmbH & Co. KG, PO Box 1103, D-31849 Aerzen, Germany. *Electromagnetic clutch and brake INTORQ 14.105 and INTORQ 14.115*, 2005.
- [26] Hübner Elektromaschinen GmbH, Planufer 92 b, D-10967 Berlin, Germany. *HEAG 164-15 Differenzverstärker*, 2006.
- [27] Hübner Elektromaschinen GmbH, Planufer 92 b, D-10967 Berlin, Germany. *ACC 70 ACC 74 Ferraris Acceleration Sensor*, March 2007.
- [28] burster Präzisionsmesstechnik GmbH & Co. KG, Talstr.1-5, D-76593 Gernsbach, Germany. *Hochpräzisions-Kraftsensoren Serien 85040 und 85070*, 2008.